
Edge-augmented Graph Transformers: Global Self-attention is Enough for Graphs

Md Shamim Hussain

Department of Computer Science
Rensselaer Polytechnic Institute
110 8th St.
Troy/NY, USA
hussam4@rpi.edu

Mohammed J. Zaki

Department of Computer Science
Rensselaer Polytechnic Institute
110 8th St.
Troy/NY, USA
zaki@cs.rpi.edu

Dharmashankar Subramanian

IBM Research
dharmash@us.ibm.com

Abstract

Transformer neural networks have achieved state-of-the-art results for unstructured data such as text and images but their adoption for graph-structured data has been limited. This is partly due to the difficulty of incorporating complex structural information in the basic transformer framework. We propose a simple yet powerful extension to the transformer – residual edge channels. The resultant framework, which we call Edge-augmented Graph Transformer (EGT), can directly accept, process and output structural information as well as node information. It allows us to use global self-attention, the key element of transformers, directly for graphs and comes with the benefit of long-range interaction among nodes. Moreover, the edge channels allow the structural information to evolve from layer to layer, and prediction tasks on edges/links can be performed directly from the output embeddings of these channels. In addition, we introduce a generalized positional encoding scheme for graphs based on Singular Value Decomposition which can improve the performance of EGT. Our framework, which relies on global node feature aggregation, achieves better performance compared to Convolutional/Message-Passing Graph Neural Networks, which rely on local feature aggregation within a neighborhood. We verify the performance of EGT in a supervised learning setting on a wide range of experiments on benchmark datasets. Our findings indicate that convolutional aggregation is not an essential inductive bias for graphs and global self-attention can serve as a flexible and adaptive alternative. Our code is publicly available at <https://github.com/shamim-hussain/egt>.

1 Introduction

Graph-structured data are ubiquitous in different areas ranging from communication networks, molecular structures, citation networks, knowledge bases and social networks. Due to the flexibility of the structural information in graphs, they are powerful tools for the compact and intuitive representation of data originating from a very wide range of sources. Although Graphs are more expressive in terms of structural representation than regularly arranged sequential, time-series and grid-like data (e.g., text, audio, video), this flexibility comes at the cost of added complexity in processing and learning from graph-structured data. Recently the go-to solution for deep representation learning on graphs has been Graph Neural Networks (GNNs) [1, 2]. The most commonly used GNNs follow a

convolutional pattern whereby each node in the graph updates its state based on that of its neighbors [3, 4], in each layer. On the other hand, in the field of natural language processing, self-attention based transformer neural networks [5] have achieved great success in a wide range of tasks such as language understanding, machine translation and question answering, displacing convolutional and recurrent neural networks to become the new de-facto standard. Although originally conceived for sequential data, more specifically textual data [6, 7], the success of transformers has translated to other forms of unstructured data in different domains such as audio [8, 9] and images [10, 11] and also on different (classification/generation, supervised/unsupervised) tasks, often establishing a new state of the art. However, transformers differ from convolutional and recurrent neural networks in a very important way – the internal arrangement of the data, i.e., the sequential or grid-like pattern of positions does not directly dictate how it is processed by a transformer. Rather, the positional information is treated as an input to the network in the form of positional encodings. Information is propagated among different positions only via the global self-attention mechanism, which is agnostic to the internal arrangement of the data. Due to this property of global self-attention, distant points in the data can interact with each other as efficiently as nearby points. However, the highly arbitrary nature of structure in graphs makes it difficult to represent the position of each node only in terms of positional encodings. Methods like Graph-BERT [12] need to employ multiple types of relative positional encodings and skip connections to efficiently incorporate the structural information within the node embeddings. However, node positional encodings are not powerful enough to generalize to graphs of arbitrary complexities in terms of the interconnectivity of nodes. Also, it is not clear how edge features could be incorporated in terms of node embeddings.

We introduce a new addition to the transformer, namely residual edge channels – a pathway that can facilitate both the input and the processing of structural information. This is a simple yet powerful extension to the transformer framework in that it allows the network to directly process graph-structured data. This addition is also very general in the sense that, it facilitates the input of structural information of arbitrary form, including edge features, and can handle different variants of graphs such as directed and weighted graphs in a uniform manner. Additionally, we introduce a form of generalized positional encoding method for all variants of graphs (including directed and weighted) based on Singular Value Decomposition (SVD) of the adjacency matrix. Our framework can match and often exceed the results of widely used Graph Convolutional Networks (GCNs) on datasets of moderate to large sizes, in supervised benchmarking tasks while maintaining a similar number of parameters. But, our architecture deviates significantly from GCNs in that it does not impose any strong inductive bias such as convolution, on the feature aggregation process. We rely solely on the global self-attention mechanism to learn how best to use the structural information, rather than constraining it to a fixed pattern. Additionally, the structural information can evolve over layers and the network can potentially form new structures. Any prediction on the structure of the graph, such as link prediction or edge classification, can be done directly from the outputs of edge channels. However, these channels do add to the quadratic computational and memory complexity of global self-attention, with respect to the number of nodes, which restricts us to moderately large graphs.

Our experimental results indicate that given enough data and with the proposed edge channels, the model can utilize global self-attention to learn the best aggregation pattern for the task at hand. Thus, our results indicate that following a fixed convolutional aggregation pattern whereby each node is limited to aggregating its closest neighbors (based on adjacency, distance, intimacy, etc.) is not an essential inductive bias. With the flexibility of global self-attention, the network can learn to

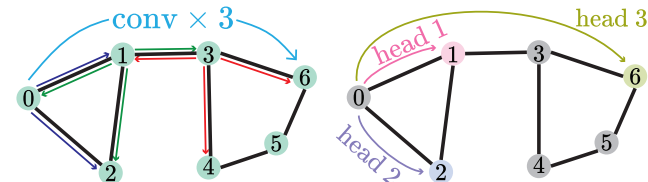


Figure 1: A conceptual demonstration of Graph Convolution (left) and Global Self-Attention (right). It takes three stages of convolution for node 0 to aggregate node 6. With global self-attention, the model can learn to do so in a single step. The attention heads are formed dynamically for a given graph.

aggregate distant parts of the input graph in just one step (Fig. 1). This pattern is learned by the network during training rather than being imposed by design, so it increases the expressivity of the model. Also, this aggregation pattern is dynamic and can adapt to each specific input graph. Similar findings have been reported for unstructured data such as images [11, 13, 14]. Some recent works have reported global self-attention as a means for better generalization or performance by improving the expressivity of graph convolution [15, 16]. Recently, Ying et al. [17] showed that with appropriate encodings, transformers can perform well in representation learning on molecular graphs. But to our knowledge, we are the first to propose global self-attention as a direct replacement of graph convolution for node-level, link(edge)-level and graph-level predictions and on all forms of graph-structured data.

2 Related Work

There have been several attempts at adopting the local self-attention mechanism for graph-structured data. Methods like Graph Attention Networks (GAT) [18] and Graph Transformer (GT) [19] constrain the self-attention mechanism to local neighborhoods of each node only. Several works have attempted to adopt the global self-attention mechanism for graphs as well. Graph-BERT [12] uses a modified transformer framework on a sampled linkless subgraph (i.e., only node representations are processed) around a target node. Since the nodes don't inherently bear information about their interconnectivity, Graph-BERT uses several types of relative positional encodings to embed the information about the edges within a subgraph. GROVER [20] used a modified transformer architecture with queries, keys and values produced by Message-Passing Networks, which indirectly incorporate the input structural information. This framework was used to perform self-supervised learning on molecular graphs. Graphomer [17] and Graph Transformer [21] directly adopt the scaled dot product based global attention mechanism of transformers. Graphomer incorporates the existing edges in the graph as an attention bias, whereas Graph Transformer does so with a weighted average of learned and existing edges. However, these architectures were specialized for a given graph learning setting (e.g., regression on molecular graphs). Unlike these works, we directly incorporate graph structure into the transformer model via the edge channels and propose a general-purpose learning framework for graphs based only on the global self-attention mechanism, free of the strong inductive bias of convolution. Apart from being used for node feature aggregation, attention has also been used to form metapaths in heterogeneous graphs [22, 23].

Positional encodings have been used for GNNs to embed global positional information within individual nodes and to distinguish isomorphic nodes and edges [24, 25]. Murphy et al. [24] use one-hot vectors corresponding to node indices. Graph-BERT [12] uses three types of positional encodings: Weisfeiler-Lehman, intimacy, and hop based positional encodings. Among these, the last two encoding schemes are relative in nature and are only relevant when performing prediction tasks on a node of interest within a sampled subgraph. Inspired by matrix factorization based node embedding methods for graphs [26], Dwivedi et al. [27] proposed to use the k smallest non-trivial eigenvectors of the Laplacian matrix of the graph as positional encodings. However, since the Laplacian eigenvectors can be complex-valued for directed graphs, this method is more relevant for undirected graphs which have symmetric Laplacian matrices. Our SVD-based positional encoding method is more general since it generates real-valued encodings for any graph structural matrix and all variants of graphs (e.g., directed, weighted).

3 Network Architecture

3.1 Edge-augmented Graph Transformer

The EGT architecture (Fig. 2) extends the original transformer [5] architecture. The transformer treats the input embeddings as a multiset, which is ideal for processing the node embeddings in a graph. Thus, we call the residual channels present in the original transformer architecture *node channels*. These channels transform a set of input node embeddings $\{h_1^0, h_2^0, \dots, h_N^0\}$ into a set of output node embeddings $\{(h_1^L)_{final}, (h_2^L)_{final}, \dots, (h_N^L)_{final}\}$, where $h_i^L \in \mathbb{R}^{d_h}$, d_h is the node embeddings dimensionality, N is the number of nodes, and L is the number of layers. Our contribution to the transformer architecture is the *edge channels*, which start with an embedding for each pair of nodes. Thus, there are $N \times N$ input edge embeddings $e_{11}^0, e_{12}^0, \dots, e_{1N}^0, e_{21}^0, \dots, e_{NN}^0$ where, $e_{ij}^l \in \mathbb{R}^{d_e}$, d_e

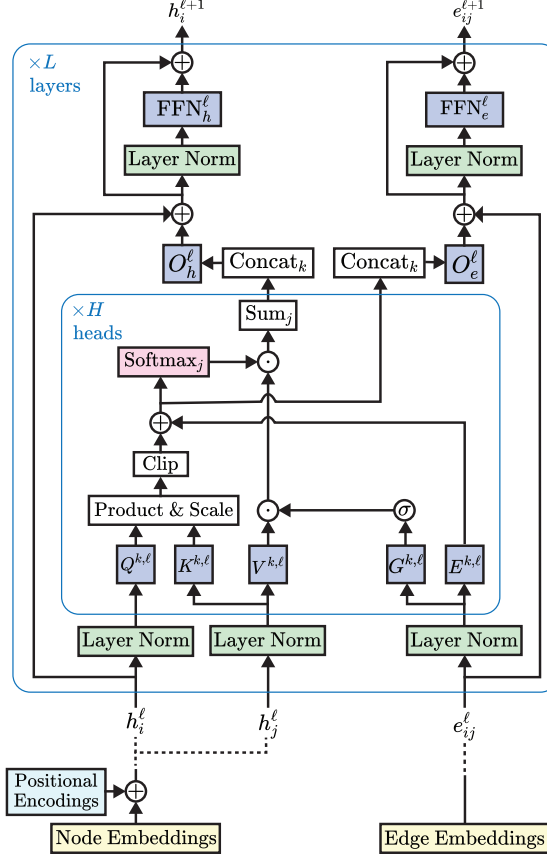


Figure 2: EGT: Edge-augmented Graph Transformer

is the edge embeddings dimensionality. The input edge embeddings are formed from graph structural matrices and edge features. We define a graph structural matrix as any matrix with dimensionality $N \times N$, which can completely or partially define the structure of a graph (e.g., adjacency matrix, distance matrix, Laplacian matrix). The edge embeddings are updated by EGT in each layer and finally, it produces a set of output edge embeddings $(e_{ij}^L)_{final}$ (for $1 \leq i, j \leq N$) from which structural predictions such as edge labeling and link prediction can be performed.

Each layer in the transformer encoder consists of two sublayers. The key component of the transformer is the multihead self-attention mechanism which takes place in the first sublayer. In the ℓ 'th layer and for the k 'th attention head, this can be expressed as:

$$\text{Attn}(\mathbf{Q}_h^{k,\ell}, \mathbf{K}_h^{k,\ell}, \mathbf{V}_h^{k,\ell}) = \tilde{\mathbf{A}}^{k,\ell} \mathbf{V}_h^{k,\ell} \quad (1)$$

$$\text{Where, } \tilde{\mathbf{A}}^{k,\ell} = \text{softmax}(\hat{\mathbf{A}}^{k,\ell}) \quad (2)$$

$$\hat{\mathbf{A}}^{k,\ell} = \frac{\mathbf{Q}_h^{k,\ell} (\mathbf{K}_h^{k,\ell})^T}{\sqrt{d_k}} \quad (3)$$

where $\mathbf{Q}_h^{k,\ell}, \mathbf{K}_h^{k,\ell}, \mathbf{V}_h^{k,\ell} \in \mathbb{R}^{N \times d_k}$ are the concatenation of the keys, queries and values formed by learned linear transformations of the node embeddings, i.e., $\mathbf{Q}^{k,\ell} h_i^\ell, \mathbf{K}^{k,\ell} \hat{h}_i^\ell, \mathbf{V}^{k,\ell} \hat{h}_i^\ell$, respectively. Here, H is the number of attention heads, and $d_k = d_h/H$ is the dimensionality of the query, key and value vectors. $\hat{\mathbf{A}}^{k,\ell} \in \mathbb{R}^{N \times N}$ are the attention matrices, formed from the scaled dot products $\hat{\mathbf{A}}^{k,\ell}$. We can compare each attention matrix with a row-normalized adjacency matrix of a directed weighted complete graph. They dictate how the node features in a graph are aggregated, similar to GCN [3]. Unlike the input graph, these graphs are dynamically formed by the attention mechanism. However, the basic transformer does not have a direct way to incorporate the input structure (existing edges) while forming these weighted graphs, i.e., the attention matrices. Also, these dynamic graphs

are collapsed immediately after the aggregation process is done. To remedy the first problem we let the edge channels participate in the aggregation process as follows (as shown in Fig. 2):

$$\tilde{\mathbf{A}}^{k,\ell} = \text{softmax}(\hat{\mathbf{H}}^{k,\ell}) \odot \sigma(\mathbf{G}_e^{k,\ell}) \quad (4)$$

$$\text{Where, } \hat{\mathbf{H}}^{k,\ell} = \text{clip}(\tilde{\mathbf{A}}^{k,\ell}) + \mathbf{E}_e^{k,\ell} \quad (5)$$

where \odot denotes elementwise product. $\mathbf{E}_e^{k,\ell}, \mathbf{G}_e^{k,\ell} \in \mathbb{R}^{N \times N}$ are concatenations of the learned linear transformed edge embeddings, i.e., $\mathbf{E}^{k,\ell} \hat{e}_{ij}^{\ell}, \mathbf{G}^{k,\ell} \hat{e}_{ij}^{\ell}$ respectively. $\mathbf{E}_e^{k,\ell}$ is a bias term added to the scaled dot product. It lets the edge channels influence the attention process. $\mathbf{G}_e^{k,\ell}$ drives the sigmoid $\sigma(\cdot)$ function and lets the edge channels also gate the values before aggregation. The scaled dot product is clipped to a limited range which leads to better numerical stability. We used a range of $[-5, +5]$.

To let the structural information evolve from layer to layer, the edge embeddings are updated by a learnable linear transformation of the inputs to the softmax function. The outputs of the attention heads are also mixed by a linear transformation. To facilitate training deep networks, Layer Normalization (LN) [28] and residual connections [29] are used. We adopted the Pre-Norm architecture whereby normalization is done immediately before the weighted sublayers [30] rather than after, because of its better optimization characteristics. So, $\hat{h}_i^{\ell} = \text{LN}(h_i^{\ell-1})$, $\hat{e}_{ij}^{\ell} = \text{LN}(e_{ij}^{\ell-1})$. The residual updates can be expressed in an elementwise manner as:

$$\hat{h}_i^{\ell} = h_i^{\ell-1} + \mathbf{O}_h^{\ell} \parallel \sum_{k=1}^H \tilde{\mathbf{A}}_{ij}^{k,\ell} (\mathbf{V}^{k,\ell} \hat{h}_i^{\ell}) \quad (6)$$

$$\hat{e}_{ij}^{\ell} = e_{ij}^{\ell-1} + \mathbf{O}_e^{\ell} \parallel \hat{\mathbf{H}}_{ij}^{k,\ell} \quad (7)$$

Here, \parallel denotes concatenation. $\mathbf{O}_h^{\ell} \in \mathbb{R}^{d_h \times d_h}$ and $\mathbf{O}_e^{\ell} \in \mathbb{R}^{d_e \times H}$ are the learned output projection matrices, with edge embeddings dimensionality d_e and H attention heads.

The attention sublayer is followed by a feed-forward sublayer which applies a pointwise non-linear transformation on the embeddings. This is achieved by two consecutive pointwise fully connected linear layers with a non-linearity such as ELU [31] in between. The updated embeddings are $h_i^{\ell} = \hat{h}_i^{\ell} + \text{FFN}_h^{\ell}(\text{LN}(\hat{h}_i^{\ell})), e_i^{\ell} = \hat{e}_{ij}^{\ell} + \text{FFN}_e^{\ell}(\text{LN}(\hat{e}_{ij}^{\ell}))$. The Pre-Norm architecture also ends with a layer normalization over the final embeddings as $(h_i^L)_{final} = \text{LN}(h_i^L), (e_{ij}^L)_{final} = \text{LN}(e_{ij}^L)$.

3.2 SVD-based Positional Encodings

While applying the transformer on regularly arranged data such as sequential (e.g., text) and grid-like (e.g., images) data it is customary to use sinusoidal positional encodings introduced by Vaswani et al. [5]. However, the arbitrary nature of structure in graphs makes it difficult to devise a consistent positional encoding scheme. We propose a form of positional encoding based on precalculated SVD of the graph structural matrices. We use the largest r singular values and corresponding left and right singular vectors to form our positional encodings. Primarily, we use the adjacency matrix \mathbf{A} (with self-loops) as the graph structural matrix, but it can be generalized to other structural matrices since the SVD of any real matrix produces real singular values and vectors.

$$\mathbf{A} \xrightarrow{\text{SVD}} \mathbf{U} \Sigma \mathbf{V}^T = (\mathbf{U} \sqrt{\Sigma}) \cdot (\mathbf{V} \sqrt{\Sigma})^T = \hat{\mathbf{U}} \hat{\mathbf{V}}^T \quad (8)$$

$$\hat{\Gamma} = \hat{\mathbf{U}} \parallel \hat{\mathbf{V}} \quad (9)$$

Where $\mathbf{U}, \mathbf{V} \in \mathbb{R}^{N \times r}$ matrices contain the r left and right singular vectors as columns, respectively, corresponding to the top r singular values in the diagonal matrix $\Sigma \in \mathbb{R}^{r \times r}$. Here, \parallel denotes concatenation along columns. From (8) we see that the dot product between i 'th row of $\hat{\mathbf{U}}$ and j 'th row of $\hat{\mathbf{V}}$ can approximate \mathbf{A}_{ij} which denotes whether there is an edge between nodes i and j . Thus, the rows of $\hat{\Gamma}$, namely $\hat{\gamma}_1, \hat{\gamma}_2, \dots, \hat{\gamma}_N$, each with dimensionality $\hat{\gamma}_i \in \mathbb{R}^{2r}$, bear denoised information about the edges and can be used as positional encodings. Note that this form of representation based on dot product is consistent with the scaled dot product attention used in the transformer framework. Since the signs of corresponding pairs of left and right singular vectors can be arbitrarily flipped, we

can randomly flip the signs of $\hat{\gamma}_i$ during training. This can be thought of as a form of data augmentation that makes the model more robust to the input positional encodings that can be especially important for smaller datasets on which the model tends to overfit. Instead of directly adding $\hat{\gamma}_i$ to the input embeddings of the node i , we add a projection $\gamma_i = \mathbf{W}_{enc}\hat{\gamma}_i$, where $\mathbf{W}_{enc} \in \mathbb{R}^{d_h \times 2r}$ is a learned projection matrix. This heuristically leads to better results. Since our architecture directly takes structure as input via the edge channels, the inclusion of positional encodings is optional for most tasks. However, positional encodings can help distinguish isomorphic nodes [32]. Thus, they make the architecture more expressive. Also, they encode the denoised global positional information within the node embeddings.

3.3 Embedding and Prediction

Both node and edge feature embeddings are formed by performing learnable linear transformations for continuous vector values or vector embeddings for categorical/discrete values. In the case of multiple sets of features, their corresponding embeddings are added together. When positional encodings γ_i are used, they are added to the input node embeddings. The edge embeddings are formed by adding together the embeddings from the graph structural matrix and the input edge feature embeddings (when present). For non-existing edges, a masking value/vector is used in the place of an edge feature. As input structural matrix, we use the unnormalized graph adjacency matrix with self-loops \mathbf{A} where $\mathbf{A}_{ij} \in \{0, 1\}$, or the distance matrix clipped up to k -hop distance, i.e., $\mathbf{D}^{(k)}$ where $\mathbf{D}_{ij}^{(k)} \in \{0, 1, \dots, k\}$. We use vector embeddings of the discrete values contained in these matrices.

For node and edge classification/regression tasks, we apply a few final MLP layers on the node and edge embeddings, respectively, to produce the final output. For graph-level classification/regression we adopt one of two different methods. In *global average pooling* method, all the output node embeddings are averaged to form a graph-level embedding, on which final linear layers are applied. In *virtual nodes* method, q new virtual nodes with learnable input embeddings $h_{N+1}^0, h_{N+2}^0, \dots, h_{N+q}^0$ are passed through the EGT along with existing node embeddings. There are also q different learnable edge embeddings \tilde{e}_i which are used as follows – the edge embedding between a virtual node i and existing graph node j is assigned $e_{ij}^0 = e_{ji}^0 = \tilde{e}_i$, and the edge embeddings between two virtual nodes i, j , are assigned $e_{ij}^0 = e_{ji}^0 = \frac{1}{2}(\tilde{e}_i + \tilde{e}_j)$. Finally, the graph embedding is formed by concatenating the output node embeddings of the virtual nodes. This method is more flexible and better suited for larger models.

For smaller datasets, we found that adding a secondary *distance prediction objective* alongside the graph-level prediction task in a multi-task learning setting serves as an effective means of regularization and thus improves the generalization of the trained model. This self-supervised objective is reminiscent of the unsupervised link prediction objective often used to pre-train GNNs to form node embeddings. In our case, we take advantage of the fact that we have output edge embeddings from the edge channels (alongside the node embeddings, which are used for graph-level prediction). We thus pass the output edge embeddings through a few MLP layers and set the distance matrix up to ν -hop $\mathbf{D}^{(\nu)}$ as a categorical target. Hops greater than ν are ignored while calculating the loss. The loss from this secondary objective is multiplied by a small factor κ and added to the total loss. Note that in this case we always use the adjacency matrix, rather than the distance matrix as the input graph structural matrix so that the edge channels do not simply learn an identity transformation. We emphasize that this objective is only potentially beneficial as a regularization method for smaller datasets by guiding the aggregation process towards a Breadth-First Search pattern. In the presence of enough data, the network is able to learn the best aggregation pattern for the given primary objective, which also generalizes to unseen data.

4 Experiments and Results

We evaluate the performance of our proposed EGT architecture in a supervised and inductive setting. We focus on a diverse set of supervised learning tasks, namely, node and edge classification, and graph classification and regression.

Datasets: In the medium-scale supervised learning setting, we experimented with the benchmarking datasets proposed by Dwivedi et al. [27], namely PATTERN (14K synthetic graphs, 44-188

nodes/graph) and CLUSTER (12K synthetic graphs, 41-190 nodes/graph) for node classification, TSP (12K synthetic graphs, 50-500 nodes/graph) for edge classification, and MNIST (70K superpixel graphs, 40-75 nodes/graph), CIFAR10 (60K superpixel graphs, 85-150 nodes/graph) and ZINC (12K molecular graphs, 9-37 nodes/graph) for graph classification/regression. To evaluate the performance of EGT at large-scale we consider the graph regression task on the PCQM4M-LSC dataset [33] which contains 3.8 million molecular graphs with 1-51 nodes/graph.

Evaluation Setup: Experiments utilized AiMOS GPU supercomputer at RPI. We used the Tensorflow 2.1 numerical library. Training was done in a distributed manner on a single node with 8 NVIDIA Tesla V100 GPUs (32GB RAM/GPU), and 20-core 2.5GHz Intel Xeon CPU (768GB RAM). Masked attention was used to process mini-batches containing graphs of different numbers of nodes. This allowed us to use highly parallel tensor operations on the GPU. The results are evaluated in terms of accuracy, F1 score, or Mean Absolute Error (MAE). Hyperparameters were tuned on the validation set. Full details of hyperparameters and code are included in the Appendix.

Table 1: Experimental results on 6 benchmarking datasets from Dwivedi et al. [27]. We compare EGT against GCN [3], GraphSage [34], GIN [4], GAT [18], GT [19], GatedGCN [35] and PNA [36]. * indicates results are reported from [27]. The -EPE and the -SPE suffixes indicate EVD based positional encodings (by Dwivedi et al. [27]) or our SVD-based positional encodings are used respectively. DO denotes that the distance prediction objective is used in a multi-task learning setting. Results on PATTERN and CLUSTER datasets are given in terms of weighted accuracy. **Red:** best model, **Violet:** good model; for accuracy/F1 higher is better, whereas for MAE (used for ZINC) lower is better. Results not shown are not available for that method.

Model	PATTERN % Accuracy		CLUSTER % Accuracy	MNIST % Accuracy	CIFAR10 % Accuracy
	#Param ≈100K	#Param ≈500K	#Param ≈500K	#Param ≈100K	#Param ≈100K
GCN*	63.880 ± 0.074	71.892 ± 0.334	68.498 ± 0.976	90.705 ± 0.218	55.710 ± 0.381
GraphSage*	50.516 ± 0.001	50.492 ± 0.001	63.844 ± 0.110	97.312 ± 0.097	65.767 ± 0.308
GIN*	85.590 ± 0.011	85.387 ± 0.136	64.716 ± 1.553	96.485 ± 0.097	55.255 ± 1.527
GAT*	75.824 ± 1.823	78.271 ± 0.186	70.587 ± 0.447	95.535 ± 0.205	64.223 ± 0.455
GT		83.949 ± 0.303	72.139 ± 0.405		
GT-EPE		84.808 ± 0.068	73.169 ± 0.622		
GatedGCN*	84.480 ± 0.122	85.568 ± 0.088	73.840 ± 0.326	97.340 ± 0.143	67.312 ± 0.311
GatedGCN-EPE*		86.508 ± 0.085	76.082 ± 0.196		
PNA	86.567 ± 0.075			97.690 ± 0.022	70.350 ± 0.630
EGT	86.798 ± 0.032	86.825 ± 0.032	77.080 ± 0.361	97.615 ± 0.050	63.260 ± 0.735
EGT-EPE	86.827 ± 0.037	86.856 ± 0.013	76.952 ± 0.337		
EGT-SPE	86.735 ± 0.032	86.730 ± 0.036	77.909 ± 0.245	97.573 ± 0.068	63.968 ± 1.252
EGT-SPE + DO				97.722 ± 0.222	67.004 ± 0.624

Model	TSP F1		ZINC MAE		
	#Param ≈100K	#Param ≈500K	#Param ≈100K	#Param ≈500K	
GCN*	0.630 ± 0.001		0.459 ± 0.006	0.367 ± 0.011	
GraphSage*	0.665 ± 0.003		0.468 ± 0.003	0.398 ± 0.002	
GIN*	0.656 ± 0.003		0.387 ± 0.015	0.526 ± 0.051	
GAT*	0.671 ± 0.002		0.475 ± 0.007	0.384 ± 0.007	
GT				0.264 ± 0.008	
GT-EPE				0.226 ± 0.014	
GatedGCN*	0.808 ± 0.003	0.838 ± 0.002	0.375 ± 0.003	0.282 ± 0.015	
GatedGCN-EPE*				0.214 ± 0.013	
PNA			0.188 ± 0.004		
EGT	0.807 ± 0.004	0.845 ± 0.001	0.370 ± 0.016	0.302 ± 0.023	
EGT-EPE			0.336 ± 0.029	0.242 ± 0.010	
EGT-SPE	0.810 ± 0.003	0.844 ± 0.002	0.277 ± 0.019	0.223 ± 0.007	
EGT-SPE + DO			0.171 ± 0.013	0.154 ± 0.011	

4.1 Medium-scale Performance

For the benchmarking datasets, we follow the training setting suggested by Dwivedi et al. [27] and evaluate the performance of EGT for a given parameter budget. Comparative results are presented in Table 1. All datasets except PATTERN and CLUSTER include edge features. Among the models, only GT, GatedGCN, PNA and our EGT take edge features as input when available, whereas others only rely on node features. Results with and without positional encodings are presented to explore their utility. Also, we compared our results against that of Laplacian eigenvectors based positional encodings proposed by Dwivedi et al. [27].

From the results, we see that EGT outperforms other GNNs (including GAT and GT which use local self-attention rather than global) on all datasets except CIFAR10 where it is second to PNA. Note that PNA, which uses a set of sophisticated local aggregators, has an advantage over the basic form of global self-attention which simply performs a weighted aggregation. We leave the task of devising more sophisticated global aggregators as a future problem. The edge channels allow us to use the distance prediction objective in a multi-task learning setting, which helps the model overcome the overfitting problem on CIFAR10, ZINC and MNIST. Since we do not take advantage of the convolutional inductive bias our model shows various levels of overfitting on these medium-sized datasets. We posit that the EGT would further exceed the performance level of convolutional GNNs if more training data were present; we confirm this in the next section. Also, the results indicate that convolutional aggregation is not an essential inductive bias, and given enough data global attention can learn to make the best use of the structural information.

We see that the inclusion of SVD-based positional encodings leads to an improvement in most cases, although not for PATTERN and TSP. This is consistent with our proposal that positional encodings are optional for some tasks. However, on the ZINC dataset, we see a significant improvement in the result when positional encodings are incorporated. We see that our SVD-based positional encodings performed at a similar level or better than the Laplacian eigenvectors. Note that, Laplacian eigenvectors based positional encodings only apply to datasets containing undirected graphs, e.g., PATTERN, CLUSTER and ZINC. From the validation results, we noticed that the augmentation of SVD based positional encodings by flipping the signs of the singular vectors is unnecessary for PATTERN and CLUSTER datasets.

4.2 Large-scale Performance

The results for the graph regression task on the PCQM4M-LSC dataset [33] are presented in Table 2. Note that since the test labels are no longer available, results are given over the validation set. At this large-scale setting, we utilized more advanced methods such as larger models, virtual nodes, learning rate warmup and cosine decay, dropout, and distance matrix (as input structural matrix). However, the inclusion of the SVD based positional encodings and distance prediction objective did not lead to a significant improvement (which is consistent with our assumption). We see that EGT achieves a much

Table 2: Results on PCQM4M-LSC in terms of Mean Absolute Error (lower is better). * indicates results are cited from [33]. Results for other models are cited from [17]. The suffix -VN indicates that virtual node is used [37]. GINE [38] and DeeperGCN [39] are improvements over GIN and GCN frameworks respectively. The Test results are evaluated on 5% of the test data.

Model	#Param	Train MAE	Validate MAE	Test MAE
GCN*	2.0M	0.1318	0.1684	0.1838
GIN*	3.8M	0.1203	0.1536	0.1678
GCN-VN*	4.9M	0.1225	0.1510	0.1579
GIN-VN*	6.7M	0.1150	0.1396	0.1487
GINE-VN	13.2M	0.1248	0.1430	
DeeperGCN-VN	25.5M	0.1059	0.1398	
GT	0.6M	0.0944	0.1400	
	83.2M	0.0955	0.1408	
Graphomer _{SMALL}	12.5M	0.0778	0.1264	
Graphomer	47.1M	0.0582	0.1234	0.1328
EGT _{SMALL}	11.1M	0.0728	0.1299	
EGT	48.5M	0.0270	0.1263	

lower MAE than *all* the convolutional GNNs. Its performance is slightly lower than Graphomer [17] which can be thought of as an ablated variant of our architecture but uses specialized encodings, such as centrality, spatial and edge encodings. These encodings could be used as input to EGT as well, but our focus is to demonstrate the generality of our framework rather than engineering the best method for a given task, such as regression on molecular graphs. Also, we did not perform exhaustive hyperparameter tuning to avoid overfitting the validation set. This result shows the scalability of our framework and further confirms that given enough data, global self-attention based aggregation can outperform local convolutional aggregation.

4.3 Ablation Study

Our architecture is based upon two important ideas – global self-attention based aggregation and residual edge channels. To analyze the importance of these two features, we experiment with two ablated variants of EGT: i) **EGT-Simple**: incorporates global self-attention, but instead of having dedicated residual channels for edges, it directly uses a linear transformation of the input edge embeddings e_{ij}^0 (formed from adjacency matrix and edge features) to guide the self-attention. The absence of edge channels means that the edge embeddings e_{ij} are not updated from layer to layer. So, edge classification is performed by applying MLP layers on pairwise node-embeddings. It is architecturally similar to Graphomer [17]. While it is slightly less expensive in terms of computation and memory, it still scales quadratically with the number of nodes. ii) **EGT-Constrained** limits the self-attention process to the 1-hop neighborhood of each node, which allows us to compare global self-attention to convolutional local self-attention based aggregation. Also, it only keeps track of the edge embeddings e_{ij} in the edge channels if there is an edge from node i to node j or $i = j$ (self-loop). Architecturally, this variant is similar to GT [19] and can take advantage of the sparsity of the graph to reduce computational and memory costs.

Table 3: Comparison of results for two ablated variants of EGT, along with the complete architecture. Names and suffixes bear the same meaning as in Table 1. Lower is better for MAE, and higher is better for other metrics.

Model	PATTERN % Accuracy	CLUSTER % Accuracy	MNIST % Accuracy	CIFAR10 % Accuracy
	#Param≈500K	#Param≈500K	#Param≈100K	#Param≈100K
EGT	86.825 ± 0.032	77.080 ± 0.361	97.615 ± 0.050	63.260 ± 0.735
EGT-SPE	86.729 ± 0.036	77.626 ± 0.520	97.573 ± 0.068	63.968 ± 1.252
EGT-SPE + DO			97.722 ± 0.222	67.004 ± 0.624
EGT-Simple	86.794 ± 0.020	76.989 ± 0.102	97.940 ± 0.192	62.840 ± 0.648
EGT-Simple-SPE	86.746 ± 0.055	76.858 ± 0.218	97.487 ± 0.438	63.260 ± 0.569
EGT-Constrained	84.267 ± 0.555	74.532 ± 0.280	96.753 ± 0.297	63.165 ± 0.139
EGT-Constrained-SPE	86.629 ± 0.041	76.701 ± 0.257	96.823 ± 0.204	65.192 ± 0.475

Model	TSP F1	ZINC MAE	ZINC-FULL MAE	PCQM4M-LSC MAE
	#Param≈500K	#Param≈500K	#Param≈500K	#Param≈48M
EGT	0.845 ± 0.001	0.302 ± 0.023	0.051 ± 0.002	0.1263
EGT-SPE	0.844 ± 0.002	0.223 ± 0.007	0.042 ± 0.005	
EGT-SPE + DO		0.154 ± 0.011		
EGT-Simple	0.818 ± 0.002	0.383 ± 0.025	0.056 ± 0.001	0.1276
EGT-Simple-SPE	0.819 ± 0.002	0.266 ± 0.034	0.049 ± 0.002	
EGT-Constrained	0.846 ± 0.001	0.232 ± 0.010	0.063 ± 0.004	0.1328
EGT-Constrained-SPE	0.846 ± 0.001	0.174 ± 0.004	0.051 ± 0.003	

From the results in Table 3 we see that full EGT performs the best (first three rows), except for MNIST with slightly lower results. EGT-Simple can come close to EGT, but is especially subpar when the targeted task is related to edges (e.g., edge classification on the TSP dataset) due to the lack of dedicated edge channels. EGT-Constrained consistently benefits from the inclusion of positional encodings, indicating that they are more important when we perform local aggregation because they serve to provide global information to the nodes. On CIFAR10 and ZINC, it achieves better results

than pure EGT due to its convolutional inductive bias but loses its advantage when a regularization method such as the distance prediction objective (DO) is used or more data (larger ZINC-FULL dataset) is added. This result indicates that given enough data, global self-attention based aggregation can outperform local self-attention based aggregation.

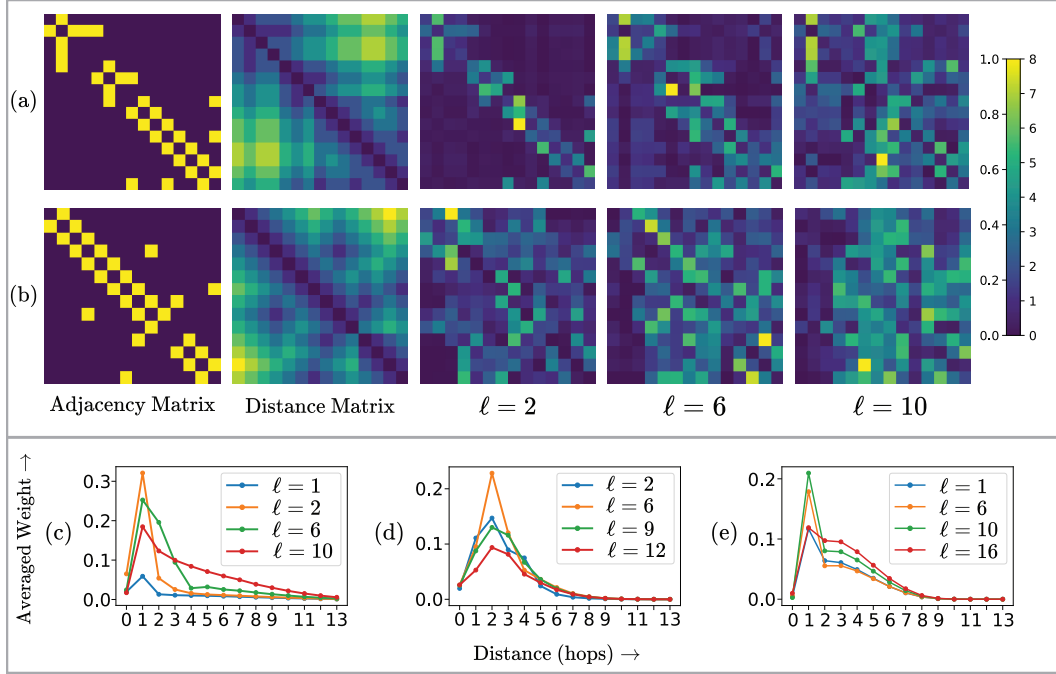


Figure 3: Above: attention patterns (attention matrices averaged over all heads and normalized between 0 and 1) for (a) ZINC and (b) PCQM4M-LSC in different layers along with the adjacency matrix and the distance matrix of the input graph (from validation set). The highest distance appearing in these inputs is 8 hops. Below: weights assigned for different hops in different layers, averaged over all heads and all nodes in all the graphs in the validation set for (c) ZINC, (d) PCQM4M-LSC, (e) TSP.

4.4 Analysis of Aggregation Patterns

To understand how global self-attention based aggregation translates to performance gains we examined the attention matrices dynamically formed by the network. These matrices dictate the weighted aggregation of the nodes and thus show how each node is looking at other nodes. This is demonstrated in Fig. 3. For the sake of visualization, we merge the attention matrices for different heads together by averaging and normalizing them to values between [0 1]. We do this for different layers at different depths of the model. We show the adjacency matrix and the distance matrix to demonstrate how far each node is looking. To make a complete analysis of each layer’s attention we also plot the weights assigned at different distances averaged over all the attention heads for all the nodes and all the graphs in a dataset. Note that a convolutional aggregation of immediate neighbors would correspond to non-zero weights being assigned to only 0/1 hop. For the ZINC dataset, from Fig. 3 (a), (c), at layer $\ell = 2$ we see that EGT approximately follows a convolutional pattern. But as we go deeper, at $\ell = 6$ the nodes start to take advantage of global self-attention to look further. Finally, at $\ell = 10$ we see highly non-local behavior. This shows why EGT has an advantage over local aggregation based convolutional networks because of its ability to aggregate global features. For PCQM4M-LSC, in Fig. 3 (b), (d), we notice such non-local aggregation patterns starting from the lowest layers. This shows why a global aggregation based model such as EGT has a clear advantage over convolutional networks (as seen in Table 2) because it would take a large number of consecutive convolutions to mimic such patterns. However, non-local aggregation is not the best strategy for all tasks. As seen from Fig. 3(e), for TSP, we see that all layers approximately follow a convolutional pattern. This also shows why EGT-Constrained achieves approximately the same result as EGT on

this dataset (Table 3). However, we emphasize the fact that EGT is able to learn this pattern even in the absence of the strong inductive bias of convolution.

5 Conclusion and Future Work

We proposed a simple extension – edge channels – to the transformer framework. We preserve the key idea, namely, global attention, while making it powerful enough to take structural information of the graph as input and also to process it and output new structural information such as new links and edge labels. One of our key findings is that the incorporation of the convolutional aggregation pattern is not an essential inductive bias for GNNs and instead the model can directly learn to make the best use of structural information. We established this claim by presenting experimental results on both medium-scale and large-scale graph learning settings and demonstrating that global self-attention based aggregation achieves superior performance in both settings. We also demonstrated that the performance improvement is directly linked to the non-local nature of aggregation of the model. In future work, we aim to evaluate the performance of EGT in transductive, semi-supervised and unsupervised settings. We also aim to explore the prospect of devising more expressive aggregators for global self-attention, similar to PNA [36]. Also, we plan to explore the prospect of reducing the computation and memory cost of our model to a sub-quadratic scale by incorporating linear attention [40, 41, 42] and sparse edge channels.

References

- [1] Marco Gori, Gabriele Monfardini, and Franco Scarselli. “A new model for learning in graph domains”. In: *Proceedings. 2005 IEEE International Joint Conference on Neural Networks, 2005*. Vol. 2. IEEE. 2005, pp. 729–734.
- [2] Franco Scarselli et al. “The graph neural network model”. In: *IEEE transactions on neural networks* 20.1 (2008), pp. 61–80.
- [3] Thomas N Kipf and Max Welling. “Semi-supervised classification with graph convolutional networks”. In: *arXiv preprint arXiv:1609.02907* (2016).
- [4] Keyulu Xu et al. “How powerful are graph neural networks?” In: *arXiv preprint arXiv:1810.00826* (2018).
- [5] Ashish Vaswani et al. “Attention is all you need”. In: *Advances in neural information processing systems*. 2017, pp. 5998–6008.
- [6] Jacob Devlin et al. “Bert: Pre-training of deep bidirectional transformers for language understanding”. In: *arXiv preprint arXiv:1810.04805* (2018).
- [7] Alec Radford et al. “Improving language understanding by generative pre-training”. In: (2018).
- [8] Rewon Child et al. “Generating long sequences with sparse transformers”. In: *arXiv preprint arXiv:1904.10509* (2019).
- [9] Naihan Li et al. “Neural speech synthesis with transformer network”. In: *Proceedings of the AAAI Conference on Artificial Intelligence*. Vol. 33. 01. 2019, pp. 6706–6713.
- [10] Mark Chen et al. “Generative pretraining from pixels”. In: *International Conference on Machine Learning*. PMLR. 2020, pp. 1691–1703.
- [11] Alexey Dosovitskiy et al. “An image is worth 16x16 words: Transformers for image recognition at scale”. In: *arXiv preprint arXiv:2010.11929* (2020).
- [12] Jiawei Zhang et al. “Graph-bert: Only attention is needed for learning graph representations”. In: *arXiv preprint arXiv:2001.05140* (2020).
- [13] Jean-Baptiste Cordonnier, Andreas Loukas, and Martin Jaggi. “On the relationship between self-attention and convolutional layers”. In: *arXiv preprint arXiv:1911.03584* (2019).
- [14] Prajit Ramachandran et al. “Stand-alone self-attention in vision models”. In: *arXiv preprint arXiv:1906.05909* (2019).
- [15] Omri Puny, Heli Ben-Hamu, and Yaron Lipman. “Global Attention Improves Graph Networks Generalization”. In: *arXiv preprint arXiv:2006.07846* (2020).
- [16] Chen Wang and Chengyuan Deng. “On the Global Self-attention Mechanism for Graph Convolutional Networks”. In: *2020 25th International Conference on Pattern Recognition (ICPR)*. IEEE. 2021, pp. 8531–8538.

[17] Chengxuan Ying et al. “Do Transformers Really Perform Bad for Graph Representation?” In: *arXiv preprint arXiv:2106.05234* (2021).

[18] Petar Veličković et al. “Graph attention networks”. In: *arXiv preprint arXiv:1710.10903* (2017).

[19] Vijay Prakash Dwivedi and Xavier Bresson. “A generalization of transformer networks to graphs”. In: *arXiv preprint arXiv:2012.09699* (2020).

[20] Yu Rong et al. “Self-supervised graph transformer on large-scale molecular data”. In: *arXiv preprint arXiv:2007.02835* (2020).

[21] Yuan Li et al. “Graph Transformer”. In: (2018).

[22] Ziniu Hu et al. “Heterogeneous graph transformer”. In: *Proceedings of The Web Conference 2020*. 2020, pp. 2704–2710.

[23] Seongjun Yun et al. “Graph transformer networks”. In: *Advances in Neural Information Processing Systems* 32 (2019), pp. 11983–11993.

[24] Ryan Murphy et al. “Relational pooling for graph representations”. In: *International Conference on Machine Learning*. PMLR. 2019, pp. 4663–4673.

[25] Balasubramaniam Srinivasan and Bruno Ribeiro. “On the equivalence between positional node embeddings and structural graph representations”. In: *arXiv preprint arXiv:1910.00452* (2019).

[26] Mikhail Belkin and Partha Niyogi. “Laplacian eigenmaps and spectral techniques for embedding and clustering.” In: *Nips*. Vol. 14. 14. 2001, pp. 585–591.

[27] Vijay Prakash Dwivedi et al. “Benchmarking graph neural networks”. In: *arXiv preprint arXiv:2003.00982* (2020).

[28] Jimmy Lei Ba, Jamie Ryan Kiros, and Geoffrey E Hinton. “Layer normalization”. In: *arXiv preprint arXiv:1607.06450* (2016).

[29] Kaiming He et al. “Deep residual learning for image recognition”. In: *Proceedings of the IEEE conference on computer vision and pattern recognition*. 2016, pp. 770–778.

[30] Ruibin Xiong et al. “On layer normalization in the transformer architecture”. In: *International Conference on Machine Learning*. PMLR. 2020, pp. 10524–10533.

[31] Djork-Arné Clevert, Thomas Unterthiner, and Sepp Hochreiter. “Fast and accurate deep network learning by exponential linear units (elus)”. In: *arXiv preprint arXiv:1511.07289* (2015).

[32] Muhan Zhang et al. “Revisiting graph neural networks for link prediction”. In: *arXiv preprint arXiv:2010.16103* (2020).

[33] Weihua Hu et al. “Ogb-lsc: A large-scale challenge for machine learning on graphs”. In: *arXiv preprint arXiv:2103.09430* (2021).

[34] William L Hamilton, Rex Ying, and Jure Leskovec. “Representation learning on graphs: Methods and applications”. In: *arXiv preprint arXiv:1709.05584* (2017).

[35] Xavier Bresson and Thomas Laurent. “Residual gated graph convnets”. In: *arXiv preprint arXiv:1711.07553* (2017).

[36] Gabriele Corso et al. “Principal neighbourhood aggregation for graph nets”. In: *arXiv preprint arXiv:2004.05718* (2020).

[37] Justin Gilmer et al. “Neural message passing for quantum chemistry”. In: *International conference on machine learning*. PMLR. 2017, pp. 1263–1272.

[38] Rémy Brossard, Oriel Frigo, and David Dehaene. “Graph convolutions that can finally model local structure”. In: *arXiv preprint arXiv:2011.15069* (2020).

[39] Guohao Li et al. “Deepergcn: All you need to train deeper gcns”. In: *arXiv preprint arXiv:2006.07739* (2020).

[40] Krzysztof Choromanski et al. “Rethinking attention with performers”. In: *arXiv preprint arXiv:2009.14794* (2020).

[41] Angelos Katharopoulos et al. “Transformers are rnns: Fast autoregressive transformers with linear attention”. In: *International Conference on Machine Learning*. PMLR. 2020, pp. 5156–5165.

[42] Imanol Schlag, Kazuki Irie, and Jürgen Schmidhuber. “Linear transformers are secretly fast weight memory systems”. In: *arXiv preprint arXiv:2102.11174* (2021).

[43] Andrew Kachites McCallum et al. “Automating the construction of internet portals with machine learning”. In: *Information Retrieval* 3.2 (2000), pp. 127–163.

- [44] Lise Getoor. “Link-based classification”. In: *Advanced methods for knowledge discovery from complex data*. Springer, 2005, pp. 189–207.
- [45] Christopher Morris et al. “Tudataset: A collection of benchmark datasets for learning with graphs”. In: *arXiv preprint arXiv:2007.08663* (2020).
- [46] Emmanuel Abbe. “Community detection and stochastic block models: recent developments”. In: *The Journal of Machine Learning Research* 18.1 (2017), pp. 6446–6531.
- [47] Radhakrishna Achanta et al. “SLIC superpixels compared to state-of-the-art superpixel methods”. In: *IEEE transactions on pattern analysis and machine intelligence* 34.11 (2012), pp. 2274–2282.
- [48] Yann LeCun et al. “Gradient-based learning applied to document recognition”. In: *Proceedings of the IEEE* 86.11 (1998), pp. 2278–2324.
- [49] Alex Krizhevsky, Geoffrey Hinton, et al. “Learning multiple layers of features from tiny images”. In: (2009).
- [50] John J Irwin et al. “ZINC: a free tool to discover chemistry for biology”. In: *Journal of chemical information and modeling* 52.7 (2012), pp. 1757–1768.

A Description of Datasets

In this section, we provide a detailed description of the datasets used in our experiments. We chose these datasets over more commonly used smaller datasets (e.g., Cora [43], Citeseer [44] and TU [45]), which are often used to evaluate other GNN architectures for several reasons. As mentioned by Dwivedi et al., these smaller datasets often cannot statistically distinguish the performance levels of different GNN architectures. We wanted to establish the performance level of our proposed architecture against other commonly used architectures for a set of very general machine learning tasks on graphs. Also, the numbers of nodes in the input graphs in these datasets are tractable in terms of quadratic computational and memory complexities of the proposed global self-attention based architecture.

PATTERN is a node classification dataset generated using the Stochastic Block Model [46] which poses the task of classifying the nodes in a graph into two communities. There are a total of 14K *undirected* graphs in the dataset, each with 44-188 nodes. The nodes have discrete node features associated with them but there are no edge features.

CLUSTER is also a node classification dataset generated using the Stochastic Block Model. It poses the task of classifying the nodes in each graph into 6 different clusters. There are a total of 12K *undirected* graphs in the dataset, each with 41-190 nodes. Discrete node features are present for each node. Edge features are absent.

MNIST is a graph classification dataset. It is a superpixel dataset [47] produced from the well-known MNIST dataset of handwritten digits [48]. The goal is to classify each superpixel graph into 10 different classes. Both node and edge features are present and they take continuous (vector) values. There are a total of 60K *directed* graphs, each with 40-75 nodes.

CIFAR10 is also a superpixels graph classification dataset produced from the well-known CIFAR10 dataset of tiny natural images [49]. The given task is to classify each superpixel graph into 10 different classes. Both node and edge features are present and they take continuous (vector) values. There are a total of 45K *directed* graphs, each with 85-150 nodes.

TSP is an edge classification dataset based on the Traveling Salesman Problem in the 2D plane, which is a well-studied NP-hard problem. The goal is to predict whether the edges in a k nearest neighbor graph formed from the vertices in the 2D plane, belong to the solution or not. There are 12K *directed* graphs in total, each with 50-500 nodes. Both (continuous-valued) node and edge features are present.

ZINC [50] is a dataset of real-world *undirected* molecular graphs. The goal is to predict a continuous real value (constrained solubility) from the molecular graph, i.e., this is a graph regression problem. Dwivedi et al. use a subset of 12K randomly sampled graphs, each with 9-37 nodes, for the benchmarking task from the bigger dataset. We perform our experiments on the same subset. Discrete node and edge features are present.

ZINC-FULL is the larger dataset of which ZINC is a subset. It consists of 220K *undirected* molecular graphs, each with 6-39 nodes. Although this dataset is not one of the benchmarking datasets, we use it in the ablation study.

PCQM4M-LSC [33] is a large-scale dataset of 3.8 million *undirected* molecular graphs, each with 1-51 nodes (i.e., atoms). The task is to predict a real (non-negative) valued quantum chemical property – the HOMO-LUMO energy gap for each graph (i.e., molecule). Each node and edge in each molecular graph has multiple discrete-valued features. The training dataset contains around 3 million training example graphs. The validation and the test dataset each contain around 400K graphs, however, the labels for the test dataset are no longer available.

B Training Method and Hyperparameters

B.1 Medium-scale Experiments

For medium-scale experiments on the PATTERN, CLUSTER, MNIST, CIFAR10, TSP, and ZINC (also ZINC-FULL) datasets we followed the benchmarking setting suggested by Dwivedi et al. [27]. The number of layers, the width of the node and the edge channels (L , d_h and d_e , correspondingly) were varied to get the best results on the validation set. SVD-based positional encodings, when used,

Table 4: Common hyperparameters used in medium-scale experiments.

Hyperparameter	Value
Input structural matrix	Adjacency with self-loops
Number of attention heads, H	8
Node channels FFN multiplier	2
Edge channels FFN multiplier	2
Final (two) MLP layers dimension	$d_h/2, d_h/4$
Virtual nodes	Not used
SVD encoding rank, r	8 (when used)
Dropout	Not used
Adam: initial LR	5×10^{-4}
Adam: β_1	0.9
Adam: β_2	0.999
Adam: ϵ	10^{-7}
Reduce LR by factor	0.5
Minimum LR	5×10^{-6}
LR warmup	Not used
Cosine decay	Not used

Table 5: Specific hyperparameters used for each dataset in medium-scale experiments.

Hyperparameter	PATTERN	CLUSTER	MNIST	CIFAR10	TSP	ZINC	ZINC-FULL
Batch size	128	128	128	128	8	128	128
Maximum no. of epochs	200	200	200	200	100	600	200
Reduce LR patience (epochs)	10	10	10	10	5	20	5
SVD encodings augmentation*	No	No	Yes	Yes	Yes	Yes	No
No- of Laplacian eigenvectors*	2	20				8	
Distance objective: ν^*			3 hops	3 hops		3 hops	
Distance objective: κ^*			5×10^{-4}	5×10^{-4}		5×10^{-2}	
For #Param≈100K							
Number of layers, L	4	4	4	4	4	4	
Node channels width, d_h	64	64	64	64	64	48	
Edge channels width, d_e	8	8	8	8	8	48	
For #Param≈500K							
Number of layers, L	16	16			16	10	10
Node channels width, d_h	64	64			64	64	64
Edge channels width, d_e	8	8			8	64	64

are formed from $r = 8$ singular values/vectors. We used the Adam optimizer and reduce the learning rate by a factor of 0.5 if the validation loss does not improve for a given number of epochs (Reduce LR when validation loss plateaus). We noticed a considerable amount of overfitting on some datasets if we kept training the network indefinitely, so we keep track of the validation loss at the end of each epoch and pick the set of weights that produces the least validation loss. Each experiment (training and evaluation) was run 4 times with 4 different random seeds and the results were used to calculate the mean and standard deviations of the metric. The common hyperparameters and methods for all datasets are given in Table 4, whereas the hyperparameters which are specific for each dataset are given in Table 5.

B.2 Large-scale Experiments

For a fair comparison on the PCQM4M-LSC dataset, we did not tune the hyperparameters exhaustively on the validation set in order to prevent overfitting the validation set. Note that the validation set contains enough data (400K molecular graphs) to make a fair comparison. In presence of a large amount of training data, we were able to train large models. We found that it is essential to use learning rate warmup to train bigger models. Also, we found that the use of virtual nodes to collect more graph-level information and the use of distance matrix instead of the adjacency matrix is beneficial at these large-scale. Note that, these additions did not result in any significant improvement for smaller datasets. To improve generalization we also used dropout (in the node channels only). We did not use the validation set to stop training, rather trained all models for a fixed number (1 million) of gradient update steps, including learning rate warmup steps (60K steps) followed by a cosine decay to a learning rate of zero. The hyperparameters are shown in Table 6.

Table 6: Hyperparameters used on PCQM4M-LSC.

Hyperparameter	Value
Input structural matrix	Distance matrix (clipped up to 16 hops)
Number of attention heads, H	32
Node channels FFN multiplier	1
Edge channels FFN multiplier	1
Final (two) MLP layers dimension	d_h, d_h
SVD-based positional encoding	Not used
Distance prediction objective	Not used
Node channels dropout	0.1
(both MHA and FFN sublayers)	
Edge channels dropout	0
Adam: maximum LR	2×10^{-4}
Adam: β_1	0.9
Adam: β_2	0.999
Adam: ϵ	10^{-7}
Reduce LR on loss plateau	Not used
Minimum LR	0
LR warmup	60,000 steps
Cosine decay	940,000 steps
Specific to EGT_{SMALL}	
Batch size	128
Virtual nodes	4
Number of layers, L	6
Node channels width, d_h	512
Edge channels width, d_e	128
Specific to EGT	
Batch size	512
Virtual nodes	8
Number of layers, L	12
Node channels width, d_h	768
Edge channels width, d_e	128

C Details of Ablated Variants

EGT-Simple: EGT-simple uses global self-attention, but does not have dedicated residual channels for updating pairwise information (edges). The input edge embeddings (formed from graph structural matrix and edge features) directly participate in the aggregation process as follows:

$$\tilde{\mathbf{A}}^{k,\ell} = \text{softmax}(\hat{\mathbf{H}}^{k,\ell}) \odot \sigma(\mathbf{G}_0^{k,\ell}) \quad (10)$$

$$\text{Where, } \hat{\mathbf{H}}^{k,\ell} = \text{clip}(\hat{\mathbf{A}}^{k,\ell}) + \mathbf{E}_0^{k,\ell} \quad (11)$$

$\mathbf{E}_0^{k,\ell}, \mathbf{G}_0^{k,\ell} \in \mathbb{R}^{N \times N}$ are directly formed by concatenations of the learned linear transformed input edge embeddings, i.e., $\mathbf{E}^{k,\ell} e_{ij}^0, \mathbf{G}^{k,\ell} e_{ij}^0$ respectively. Also, the absence edge channels means that the edge embeddings e_{ij} are not updated from layer to layer. So, edge classification is performed from pairwise node embeddings and input edge features. We denote this variant as EGT-Simple since it is architecturally simpler than EGT.

For this variant, d_e denotes only the dimensionality of the input edge embeddings in the hyperparameters tables (Table 5, Table 6). During comparison, we use the same hyperparameters for this variant as the ones used for original EGT except for ZINC and ZINC-FULL datasets where we used $d_h = 80$ and $d_e = 8$ to make the number of parameters comparable.

EGT-Constrained: EGT-Constrained is a convolutional variant of EGT which limits the self-attention process to the 1-hop neighborhood of each node. It only keeps track of the edge embeddings e_{ij} in the edge channels if there is an edge from node i to node j or $i = j$ (self-loop). So, pairwise information corresponding to only the existing edges is updated by the edge channels. This architecture can be derived by taking the softmax over $j \in \mathcal{N}(i) \cup \{i\}$ while calculating the attention

weights $\tilde{\mathbf{A}}_{ij}^{k,\ell}$ and limiting the aggregation process to neighbors as:

$$\hat{h}_i^\ell = h_i^{\ell-1} + \mathbf{O}_h^\ell \left\| \sum_{k=1}^H \sum_{j \in \mathcal{N}(i) \cup \{i\}} \tilde{\mathbf{A}}_{ij}^{k,\ell} (\mathbf{V}^{k,\ell} \hat{h}_i^\ell) \right\| \quad (12)$$

Since this architecture is constrained to the existing edges we denote this as EGT-Constrained. It has the advantage that depending on the sparsity of the graph, it can have sub-quadratic computational and memory costs. However, it can be difficult to perform sparse aggregation in parallel on the GPU. Instead of sparse operations, we used masked attention to implement this architecture for faster training on datasets containing smaller graphs because we can take advantage of highly parallel tensor operations.

For this variant, d_h, d_e bear their usual meanings in the hyperparameters tables (Table 5, Table 6). We use the same hyperparameters for this variant as the ones used for original EGT.

D Additional Ablation Study

D.1 Gated vs Ungated Variants

In EGT, the edge channels participate in the aggregation process in two ways - by an attention bias and also by gating the values before they are aggregated by the attention mechanism. To verify the utility of the gating mechanism used in EGT, an ungated variant can be formulated by simplifying the aggregation process as follows:

$$\tilde{\mathbf{A}}^{k,\ell} = \text{softmax}(\hat{\mathbf{H}}^{k,\ell}) \quad (13)$$

$$\text{Where, } \hat{\mathbf{H}}^{k,\ell} = \text{clip}(\hat{\mathbf{A}}^{k,\ell}) + \mathbf{E}_e^{k,\ell} \quad (14)$$

$\mathbf{E}_e^{k,\ell} \in \mathbb{R}^{N \times N}$ is a concatenation of the learned linear transformed edge embeddings, i.e., $\mathbf{E}^{k,\ell} \hat{e}_{ij}^\ell$. Note that we omitted the sigmoid gates. The edge channels influence the aggregation process only via an attention bias. This very slightly reduces the computational cost and the number of parameters. A comparison of results of the un-gated variant with the pure EGT is shown in Table 7. From the results, we can see that the gated EGT consistently outperforms the ungated variant.

Table 7: A comparison of results of ungated EGT (EGT-U) with the pure EGT.

Model	PATTERN % Accuracy	CLUSTER % Accuracy	MNIST % Accuracy	CIFAR10 % Accuracy	TSP F1	ZINC MAE
	#Param≈500K	#Param≈500K	#Param≈100K	#Param≈100K	#Param≈500K	#Param≈500K
EGT	86.825 ± 0.032	77.080 ± 0.361	97.615 ± 0.050	63.260 ± 0.735	0.845 ± 0.001	0.302 ± 0.023
EGT-U	86.811 ± 0.040	76.811 ± 0.333	97.368 ± 0.369	61.275 ± 0.966	0.839 ± 0.002	0.371 ± 0.020

Table 8: A comparison of results for augmented (by random negation) vs. un-augmented SVD based positional encodings.

Model	PATTERN % Accuracy	CLUSTER % Accuracy	MNIST % Accuracy	CIFAR10 % Accuracy
	#Param ≈500K	#Param ≈500K	#Param ≈100K	#Param ≈100K
Un-augmented	86.730 ± 0.036	77.909 ± 0.245	96.675 ± 0.314	60.720 ± 0.883
Augmented	85.624 ± 0.642	77.626 ± 0.520	97.573 ± 0.068	63.968 ± 1.252
	TSP F1	ZINC MAE	ZINC-FULL MAE	
	#Param	#Param	#Param	
Un-augmented	0.844 ± 0.001	0.520 ± 0.008	0.042 ± 0.005	
Augmented	0.844 ± 0.002	0.223 ± 0.007	0.046 ± 0.001	

D.2 Augmentation of SVD-based Encodings

To analyze the necessity of augmentation of the SVD based positional encodings by random flipping of the signs of the singular vectors we produced results for both the augmented and un-augmented cases. These results are presented in Table 8. We see that this form of augmentation leads to an improvement in results for the MNIST, CIFAR10 and ZINC datasets. These datasets also show a high level of overfitting. Thus, the need for augmentation arises from the moderate sizes of these datasets and this necessity could be alleviated for larger datasets. To verify this, we can compare the results of the smaller ZINC dataset with the larger ZINC-FULL dataset. We see that even though it is crucial to augment the SVD based positional encodings on the smaller dataset to get a good result, this form of augmentation does not lead to an improvement of results on the bigger dataset. Note that, we observed the results on the validation sets to decide whether to perform augmentation of the SVD-based encodings or not.

E Additional Analysis of Attention Patterns

In order to better demonstrate the increasing non-local aggregation behavior with depth (deeper layers) on the ZINC dataset, in Fig. 4 (a) we demonstrate the attention patterns in all the layers in a 10 layer deep EGT model along with the adjacency matrix and the distance matrix of the input graph. Remember that attention patterns are formed by averaging attention matrices over all heads and normalizing between 0 and 1. It can be difficult to understand from the attention patterns what roles individual attention heads are playing, so in Fig. 3 (b) we show individual attention heads in

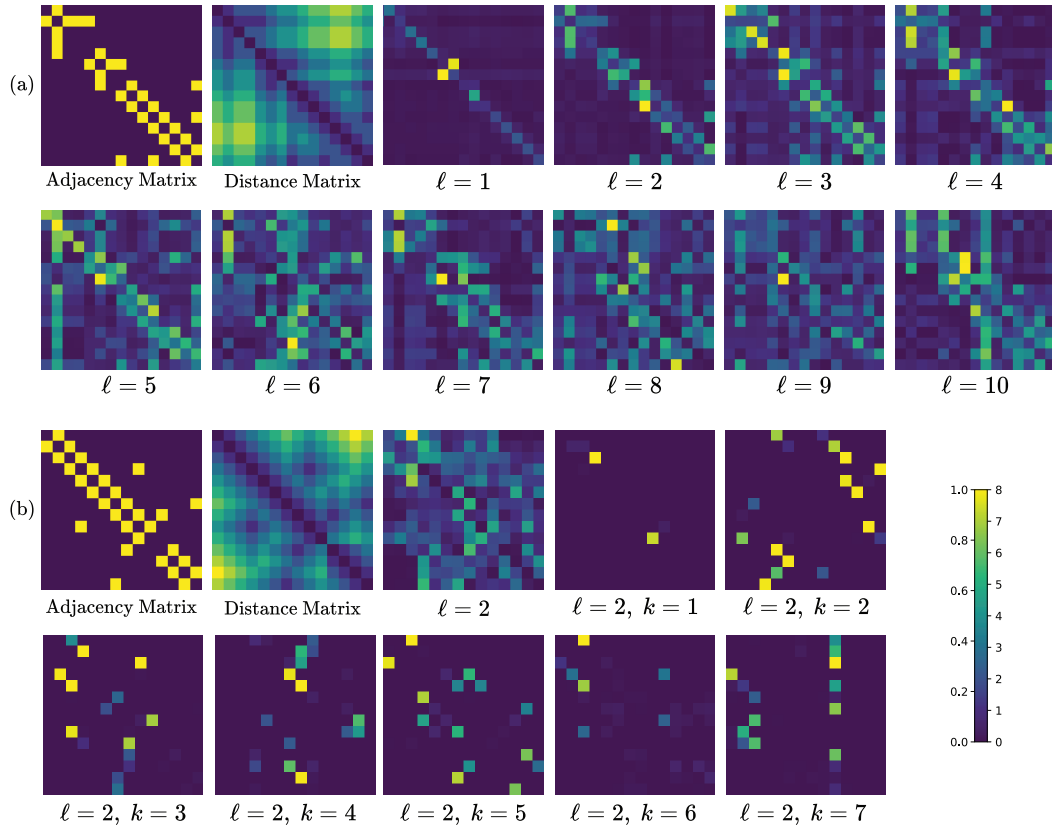


Figure 4: (a) Attention patterns (attention matrices averaged over all heads and normalized between 0 and 1) for ZINC dataset in different layers along with the adjacency matrix and the distance matrix of the input graph (from validation set). (b) Demonstration of the attention pattern with 7 individual attention heads (normalized between 0 and 1) in layer 2 for PCQM4M-LSC dataset along with the adjacency matrix, the distance matrix of the input graph (from validation set).

layer 2 of the EGT, applied on the PCQM4M-LSC dataset. We see that individual heads can be quite selective in what they aggregate, i.e., they can focus on very specific parts of the input graph. So, even though softmax attention cannot exactly assign a weight of 0 to any individual node, it can still very closely mimic a sparse aggregation pattern.